Supplementary Material

Model construction

MRI acquisition

T1-, T2- and diffusion-weighted (DW) magnetic resonance image (MRI) scans of a healthy 25-year old male subject were measured on a 3T MR scanner (Magnetom Trio, Siemens, Munich, Germany) with a 32-channel head coil. Written informed consent was obtained prior to scanning. The T1-weighted (T1w) image was acquired with an MP-RAGE pulse sequence (TR = 2300 ms, TE = 3.03 ms, TI = 1100 ms, flip angle = 8 degrees, FOV = 256 x 256 x 192 mm, voxel size = 1 x 1 x 1 mm) with fat suppression and GRAPPA parallel imaging (acceleration factor = 2). The T2-weighted (T2w) image was acquired with an SPC pulse sequence (TR = 2000 ms, TE = 307 ms, FOV = 255 x 255 x 176 mm, voxel size = 0.99 x 1.0 x 1.0 mm interpolated to 0.498 x 0.498 x 1.00 mm). The T2w sequence was adjusted such that it gives a high contrast between the different layers of the skull (figure 1(A)). The field of view of both scans captured the complete head and was cut as low as the chin.

DTI acquisition

To estimate the anisotropic conductivity tensors for the brain, we used the assumption that the conductivity tensors share eigenvectors with the measured diffusion tensors (Basser et al. 1994). Modeling of the eigenvalues will be described below. The DW images were acquired with the standard Siemens pulse sequence ep2d_diff (TR = 7700 ms, TE = 89 ms, b-value = 1000 s/mm^2, bandwidth = 2000 Hz/pixel, FOV = 220 x 220 x 141 mm, voxel size = 2.2 x 2.2 x 2.2 mm) in 61 directions equally distributed on a sphere, and 7 images were acquired with flat diffusion gradient (DW factor b = 0 (B_0-)). Additionally, seven images with flat diffusion gradient (DW factor b = 0 (B_0+)) with reversed phase and frequency encoding gradients were acquired.

Segmentation

The T2-MRI was registered onto the T1-MRI using a rigid registration approach and mutual information as a cost-function as implemented in FSL (FLIRT - FMRIB's Linear Image Registration Tool, http://www.fmrib.ox.ac.uk/fsl/flirt/index.html). The compartments skin, skull compacta and skull spongiosa were then segmented from the registered T1w and T2w images using gray-value based active contour model (Vese & Chan 2002) and thresholding techniques. These segmentations were carefully checked and corrected manually to ensure the highest possible agreement with the MR images and make sure that the different tissues form closed surfaces (figure 1(B)). Eye, neck muscle and vertebrae segmentations were added manually. The vertebrae were connected to the skull compacta. The foramen magnum and the two optic canals were correctly modeled as skull openings. The segmentation of GM and WM was extracted from brain parcellation data of the T1w image created with the freely available Freesurfer software (http://surfer.nmr.mgh.harvard.edu/).

Triangular surface meshes

The software package CURRY (CURrent Reconstruction and Imaging (CURRY), http://www.neuroscan.com/) was then used to extract high resolution triangular surface meshes of skin, eyes, skull compacta, skull spongiosa and muscle from the voxel-based segmentation volumes. The surfaces were smoothed using Taubin smoothing (Taubin & Watson 1995) to remove the blocky structure which results from the fine surface sampling of the voxels. Triangular surface meshes of all brain parcellations were made in MATLAB and refined using the package iso2mesh ((Fang & Boas 2009) http://iso2mesh.sourceforge.net/cgi-bin/index.cgi). As Freesurfer produces separate segmentations for each hemisphere, the hemispheres were attached together and (self-)intersections were removed with custom MATLAB code. The WM surface that crossed out of the GM surface especially in the inferior brain region was identified and corrected to remain inside of the GM surface. At some locations in the segmentation the brain touches the skull. To avoid resulting intersections between the GM and compacta surfaces, the complete brain was scaled down by 2% and flattened at remaining intersections.

Tetrahedral volume meshes

The smoothed surfaces (skin, compacta, spongiosa, GM, left eye, right eye, muscle) were then used to create a high quality 3D Delaunay triangulation via TetGen (TetGen: A Quality Tetrahedral Mesh Generator and a 3D Delaunay Triangulator, http://tetgen.berlios.de/). This resulted in a mesh consisting of 575k nodes and 3.54M linear tetrahedral elements (figure 1(C)). The element size in the brain was restricted to 1 mm^3. Due to the use of detailed surfaces, the elements of the skull and CSF are very small as well. A tissue index was assigned to all elements in the space between two surfaces, or inside a closed surface. We used an additional closed skull surface to label all elements within the skull surface that are not part of the brain compartments as CSF. The GM-WM surface was not used in the construction of the volume mesh, but afterwards to assign the resulting tetrahedrons within the brain compartment to either GM or WM. Surface crossing tetrahedrons were assigned on the basis of their volume ratio between the two compartments. This was necessary because inclusion of the WM surface in construction of the tetrahedral mesh would cause too many intersections in the triangular surface meshes after the cortical alterations. For this same reason the cerebellum was not included in the head model.

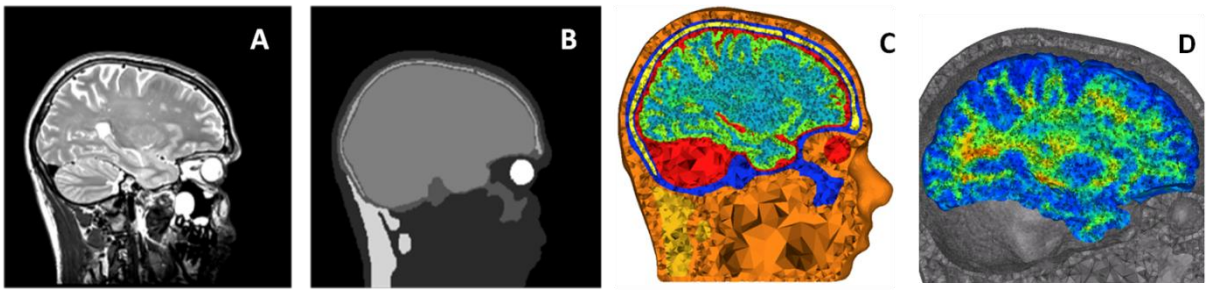

Figure 1. (A) A sagittal cut plane of the T2w MRI showing the different skull layers. (B) The same sagittal cut plane of the manually corrected segmentation including skin, skull compacta, skull spongiosa, neck muscle, eyes and one compartment for inner skull (CSF, GM and WM, before segmentation with Freesurfer). (C) Sagittal cut plane of the final tetrahedral volume mesh created with TetGen. The different tissue types are represented with different colours. The corresponding bulk conductivities are given in Table 1. (D) Sagittal cut plane of the brain mesh with the fractional anisotropy on a scale from 0 (blue) to 1 (red). The maximal fractional anisotropy value in the brain is 0.99 and the minimum is 0.

Anisotropic conductivity tensors

An important aspect of a realistic head model is tissue anisotropy (Miranda et al. 2003). For adult human subjects, the effect of brain anisotropy is mainly significant for the white matter (WM), some smaller effects can be found for the GM as well (Opitz et al. 2011).

The DW MR images were corrected for eddy current (EC) artifacts by affinely registering each directional image to the average B_0+ image using the FSL routine FLIRT. After EC correction, the gradient directions were reoriented by multiplying them with the rotational part of the transformation matrix (Leemans & Jones 2009). Another main error source for DTI analysis are the susceptibility artifacts. In order to correct for susceptibility artifacts, we used a reversed gradient approach that uses the averaged B_0+ and B_0- images to compute, using a problem-adapted multiscale nonlinear image registration procedure, smooth and diffeomorphic geometric transformations (Ruthotto et al. 2012). This approach is implemented in the freely available FAIR toolbox (Flexible Algorithms for Image Registration (FAIR), http://www.siam.org/books/fa06/). The EC and susceptibility corrections then allowed a simple rigid registration of the artifact-corrected averaged B_0 image to the T2w image (which was already registered to the T1w image in a previous step) using FLIRT. The transformation matrix obtained in this step was then used to also register the directional images to the T2w image (which is in T1 space). At this step, the corresponding gradient directions were also reoriented accordingly. From the artifact-corrected and registered DW images the diffusion tensors were then calculated using the FSL routine DTIFIT (Behrens et al. 2003). In the last step, conductivity tensors were calculated from these diffusion tensors using the volume-normalized approach as described in (Opitz et al. 2011). Next, the conductivity tensors were mapped from the MRI voxels onto the GM and WM elements of the tetrahedral head mesh described above (figure 1(D)). The normalized eigenvectors were multiplied with the conductivities of the tissues for WM and GM separately (Opitz et al. 2011). The bulk conductivity values for all tissues can be found in table 1.

Table 1. The bulk conductivity values (S/m) for all the tissue types used in the standard model.

Tissue type	Bulk conductivity (S/m)
Skin	0.465 (Wagner et al. 2004)
Skull compacta	0.007 (Akhtari et al. 2002)
Skull spongiosa	0.025 (Akhtari et al. 2002)
CSF	1.65 (Wagner et al. 2004)
Neck muscle	0.4 (Faes et al. 1999)
Eyes	1.5 (Nadeem et al. 2003)
GM	0.276 (Wagner et al. 2004)
WM	0.126 (Wagner et al. 2004)

References

Akhtari M et al., 2002. Conductivities of three-layer live human skull. *Brain topography*, 14(3), pp.151–67

Basser P J, Mattiello J & LeBihan D, 1994. MR diffusion tensor spectroscopy and imaging. *Biophysical journal*, 66(1), pp.259–67

Behrens T E J, Woolrich M W, Jenkinson M, Johansen-Berg H, Nunes R G, Clare S, Matthews P M, Brady J M, Smith S M, 2003. Characterization and propagation of uncertainty in diffusion-weighted MR imaging. *Magnetic resonance in medicine*, 50(5), pp.1077–88

Faes T J C, Van der Meij H A, De Munck J C, Heethaar R M, 1999. The electric resistivity of human tissues (100 Hz-10 MHz) a meta-analysis of review studies. *Physiological Measurements*, 1(20)

Fang Q & Boas D, 2009. Tetrahedral mesh generation from volumetric binary and gray-scale images. *International Symposium on Biomedical Imaging*, 0, pp.7–10

Leemans A & Jones D K, 2009. The B-matrix must be rotated when correcting for subject motion in DTI data. *Magnetic resonance in medicine*, 61(6), pp.1336–49

Miranda P C, Hallett M & Basser P J, 2003. The electric field induced in the brain by magnetic stimulation: a 3-D finite-element analysis of the effect of tissue heterogeneity and anisotropy. *IEEE transactions on bio-medical engineering*, 50(9), pp.1074–85

Nadeem M, Thorlin T, Gandhi O M, Persson M, 2003. Computation of electric and magnetic stimulation in human head using the 3-D impedance method. *IEEE transactions on bio-medical engineering*, 50(7), pp.900–7

Opitz A, Windhoff M, Heidemann R M, Turner R, Thielscher A, 2011. How the brain tissue shapes the electric field induced by transcranial magnetic stimulation. *NeuroImage*, 58(3), pp.849–59

Ruthotto L, Kugel H, Olesch J, Fischer B, Modersitzki J, Burger M, Wolters C H, 2012. Diffeomorphic Susceptibility Artifact Correction of Diffusion-Weighted Magnetic Resonance Images. *Phys. Med. Biol*., 57(18), pp.5715-31

Taubin G & Watson I B M T J, 1995. A Signal Processing Approach To Fair Surface Design 2 B. , pp.351–358

Vese L A & Chan T F, 2002. A Multiphase Level Set Framework for Image Segmentation Using the Mumford and Shah Model , 50(3), pp.271–293

Wagner T, Zahn M, Grodzinsky A J, Pascual-Leone A, 2004. Three-dimensional head model simulation of transcranial magnetic stimulation. *IEEE transactions on bio-medical engineering*, 51(9), pp.1586–98